Geophysical Journal International

Geophys. J. Int. (2011) **187,** 1237–1249 doi: 10.1111/j.1365-246X.2011.05196.x

Nature of remagnetization of Lower Triassic red beds in southwestern China

Chengying Liu,[1,2] Kunpeng Ge,[1,2] Chunxia Zhang,[1] Qingsong Liu,[1] Chenglong Deng[1] and Rixiang Zhu[1]

[1]*State Key Laboratory of Lithospheric Evolution, Institute of Geology and Geophysics, Chinese Academy of Sciences, Beijing* 100029*, China. E-mail: rxzhu@mail.iggcas.ac.cn*

[2]*Graduate University of the Chinese Academy of Sciences, Beijing* 100049*, China*

Accepted 2011 August 22. Received 2011 August 22; in original form 2011 February 27

SUMMARY

Widely distributed haematite-bearing red beds are an important source of palaeomagnetic field records. However, unresolved issues regarding remagnetization and inclination shallowing in red beds have questioned the reliability of the palaeomagnetic results obtained from such materials. In this study, we investigated the remagnetization mechanism in red beds from Lower Triassic sandstones in Yunnan Province, southwestern China. Our results indicate that the characteristic remanent magnetizations (ChRMs) of most samples (112/125) are dominated by only one component at temperatures 80–660 °C, with a mean direction of $D/I = 0.9/46.6^\circ$ ($k = 440.2$, $\alpha_{95} = 2.1^\circ$). The corresponding geomagnetic pole is 89.1°N, 331.7°E ($k = 338.2$, $A_{95} = 2.4^\circ$). This coincides with the present geomagnetic field, which is a strong indication that these ChRMs are remagnetized. Combined rock magnetic and microscope investigations reveal that the remagnetization is due to the acquisition of a chemical remanent magnetization (CRM) carried by authigenic maghemite and haematite. Despite the widespread remagnetization, about 7 per cent of the studied samples still record a magnetization that we consider to be primary that was isolated at high temperatures 610–660 °C, with a mean direction of $D/I = 213.3/18.6^\circ$ ($k = 16.0$, $\alpha_{95} = 11.7^\circ$). We propose that the CRM overprinting is controlled by the overlapping degree of the unblocking temperature between the CRM carried by the authigenic haematite and the primary remanent magnetization carried by the detrital haematite. Our results further suggest that microscope investigation, rock magnetic proxies for the haematite concentration and susceptibility–temperature curves are useful methods for pre-selecting samples suitable for isolating the primary remanence at this region. The linkage among the palaeomagnetic results, rock magnetic proxies and CRM remagnetization mechanism could be extended to other studies, although the detailed proxy would be different due to specific overprint process.

Key words: Remagnetization; Rock and mineral magnetism; Asia.

1 INTRODUCTION

Red beds have been extensively studied in palaeomagnetism; however, problems of remagnetization and inclination shallowing in these sediments have limited their use as a suitable candidate for palaeomagnetic studies (e.g. McCabe & Elmore 1989; Gilder *et al*. 2001). The possible carriers of the geologically stable remanence in red beds, detrital haematite and magnetite, may undergo *in situ* alteration and may be contaminated by post-depositional secondary magnetic minerals (e.g. fine pigment haematite; Collinson 1967; Cornell & Schwertmann 2003). The origin of haematite in red beds is a key issue to the timing of remanence acquisition (Walker *et al*. 1981). However, the physico-chemical conditions vary from case to case and the timing of the growth of the secondary minerals (e.g. pigment haematite and/or maghemite) is difficult to determine.

The South China Block (SCB) is one of the major tectonic units of East Asia. Despite decades of investigation, the palaeomagnetic database for south China remains sparse and subject to a degree of controversy. A major cause has been prevalent remagnetization that is widespread in this region. Several Cambrian to Triassic sedimentary units, mainly of marine sediments, exposed in the Yichang and Nanjing areas (in Hubei and Jiangsu Provinces, respectively) were studied by Kent *et al.* (1987). They concluded that widespread

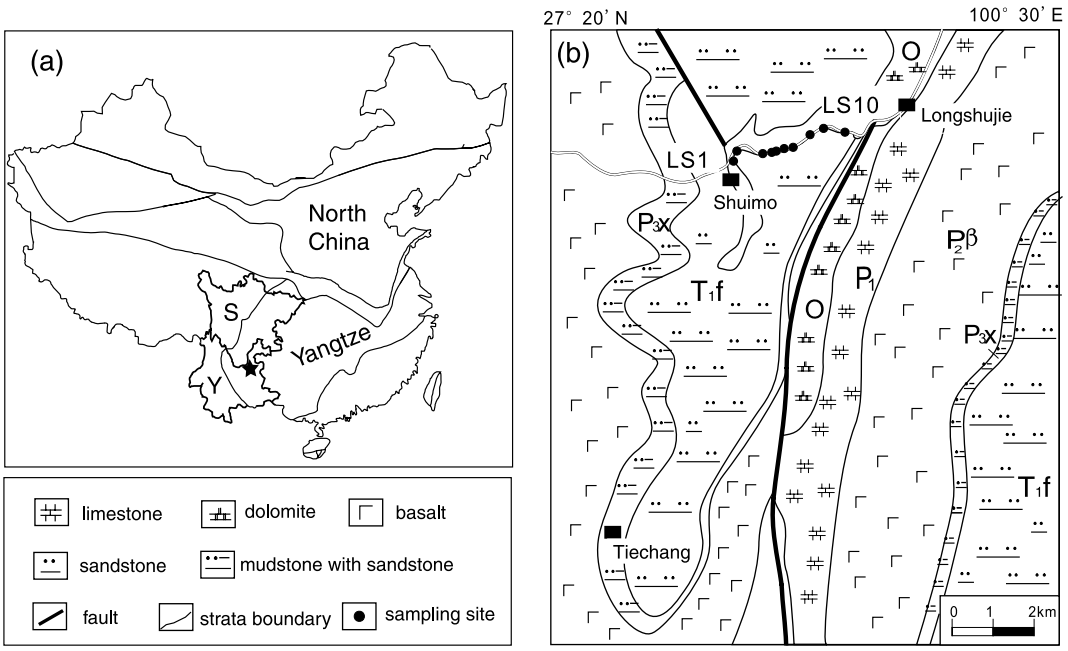

Figure 1. (a) Sketch tectonic structure of China. The star indicates the sample locality. S, Sichuan; Y, Yunnan province. (b) Geological map near the Longshujie (LS) section. Numbered dots denote the sampled sites in this study. Thick lines indicate faults. Strata: P_1 = Lower Permian; $P_2\beta$ = Permian Emeishan basalts; P_3x = Upper Permian Xuanwei Fm; T_1f = Lower Triassic Feixianguan Fm; O = Ordovician.

late Mesozoic to recent remagnetization occurred in these areas (Kent *et al.* 1987). Six Palaeozoic formations, with ages between Ordovician and Permian near Nanjing area, were also determined to have been remagnetized during the Triassic to Jurassic (Wang & Van der Voo 1993). Ages of remagnetization for marine sediments in the Guizhou and Sichuan Provinces span Carboniferous to Triassic times (Dobson & Heller 1992; Huang & Opdyke 1996; Bai *et al*. 1998). These previous studies, however, have focused mainly on marine carbonate sediments and fewer efforts have been dedicated at understanding of the nature and process of remagnetization in red beds from south China.

To better understand the remagnetization mechanism in red beds from the SCB, in this study, we have systematically investigated the Lower Triassic Feixianguan (FXG) Formation in the Longshujie (LS) profile, Yunnan Province, China. Although the natural remanent magnetizations (NRMs) for most samples is inferable as secondary, about 7 per cent of samples still carry primary remanent magnetization (PRM). The PRM was isolated by thermal demagnetization at temperatures above 610 °C. By comparing the properties of samples that were fully remagnetized to those that still retained a primary magnetization, we have gained insights into how and when the remagnetization occurred. We further define some useful criteria to pre-select red bed samples that are suitable for palaeomagnetic study.

2 GEOLOGICAL SETTING AND SAMPLING

The FXG Formation in Yunnan province is conformably underlain by the uppermost Permian Xuanwei Formation and overlain by the Lower Triassic Yongningzhen Formation. The Yongningzhen Formation is composed of limestones interbedded with mudstones and sandstones. The Xuanwei Formation is composed of sandstones, mudstones and conglomerates interbedded with coal seams, which is considered to be coeval with the Changxing Formation, which is widespread in southeast China. Within the Sichuan basin, the conformable transition from the Changxing Formation to the shallow marine or tidal flat FXG Formation is taken to be the Permian–Triassic boundary. The FXG Formation in Sichuan basin consists of distinctive red–purple limestone and mudstone, and yields reliable palaeomagnetic results (e.g. Heller *et al*. 1988; Ma & Zhang 1989; Steiner *et al*. 1989). However, when the stratigraphy is followed south into Yunnan province, the FXG Formation changes to distinctive purple–red terrestrial clastic sandstone, which suggests that the sea receded earlier than in the Sichuan basin, thus, the continental sediments were deposited above the Late Permian sediments.

The representative section of the FXG Formation in northeastern Yunnan is about 600 m thick with distinctive bright purple–red colour, and it is divisible into two members. The lower member consists of purple siltstone interbedded with fine sandstone and mudstone, and the upper member consists of purple–red thick-bedded mudstone, silty mudstone and siltstone. We collected samples from the FXG Formation near the LS village (27.31°N, 103.42°E; Fig. 1). The location of the LS profile crops out along the northeast left-lateral Xiaojiang Fault system, which is one of the main active faults during the Cenozoic in the southeastern part of the Tibetan plateau (Wang *et al*. 1998). A total of 125 samples at 10 sites were collected from limbs of an anticline–syncline system with a portable petrol-powered drill and oriented with a magnetic compass. The dip of the beds is generally shallow, ranging from 3° to 18°. The sampled massive FXG beds crop out along a road and the sample sites were within 200–500 m distance. The samples were collected at intervals of 20–50 cm, with a stratigraphic thickness of around 3 m per site. Siltstones and mudstones in both members of FXG Formation were sampled. The specimens were further processed into cylinders of 2.2 cm in length in the laboratory and fresh off-cuts were collected for rock magnetic and microscope investigations.

3 METHODS

3.1 Palaeomagnetic measurements

The NRMs were measured using a 2G-755R three-axes cryogenic magnetometer located in a magnetically shielded room in Palaeomagnetism and Geochronology Laboratory (PGL), Beijing. Specimens were subjected to stepwise thermal demagnetization in 18–20 steps up to 650 or 660 °C in an ASC TD–48 oven in the magnetically shielded room. The resulting decay pattern of the remanence was displayed in orthogonal projections (Zijderveld 1967) and the directions of the remanence components were determined using principal component analysis (Kirschvink 1980) using the PMAG program (Jones 2002). Only directions with mean angular deviations (MAD) of less than 15° were accepted. Fisher statistics (Fisher 1953) were applied to compute site mean directions. The equal-area projection of the directions is plotted with PmagPy programs (Tauxe 2010).

3.2 Rock magnetic measurements

Acquisition of isothermal remanent magnetizations (IRMs) and back-field IRMs were produced by a 2G Enterprises model 660 pulse magnetizer with fields of 1 T and reversed 300 mT, referred to as SIRM and IRM_{-300}, respectively. Anhysteretic remanent magnetizations (ARMs) were imparted in AC fields up to 100 mT with a DC bias field of 0.05 mT. To quantify the concentration of weakly magnetic but high-coercivity antiferromagnetic minerals, the 'hard' IRM ($SIRM + IRM_{-300}$)/2 (Thompson & Oldfield 1986), was evaluated. Relative abundance variations of ferrimagnetic and antiferromagnetic minerals are quantified using the *S*-ratio, which is defined as *S*-ratio = $-IRM_{-300}/SIRM$ (King & Channel 1991).

To investigate the magnetic mineralogy, temperature-dependent measurements were conducted on representative samples. Low-temperature magnetic behaviour was measured using a Quantum Design MPMS cryogenic magnetometer. Representative samples were first cooled to 10 K in a zero magnetic field, given a saturation IRM in a pulse field of 5 T, and then warmed to 300 K in a zero field. Temperature-dependent susceptibility measurements ($\chi - T$ curves) were obtained both in air and argon atmosphere (the flow rate was 50 mL min^{-1}) using a KLY-3 susceptibility bridge equipped with a CS-3 high-temperature furnace in the field of 300 A m^{-1}, with the frequency of 875 Hz.

Representative hysteresis loops and acquisition of the remanence coercivity (B_{cr}) of the bulk samples were measured on MicroMag 3900 Vibrating Sample Magnetometer (VSM; Princeton Measurements Corp., USA) at room temperature with field ranges from –1.8 to 1.8 T. The *S*-ratio, calculated from $-IRM_{-300}/IRM_{1.8T}$, is similar to the (∼2 per cent division) *S*-ratio, which suggests that the *S*-ratio is appropriate to constrain relative contributions of ferri- and antiferromagnetic minerals.

3.3 Mineralogy investigation

To investigate the microtexture directly, polished thin sections were studied under a polarizing microscope. To quantitatively confirm the minerals, X-ray diffraction (XRD) scanning from 3° to 70° using a model D/MAX-2400 X-ray diffractometer with the following parameters: Cu-Kα/40 kV/60 mA, divergence slit of 1°, scattering slit of 1°, receiving slit of 0.3 mm, continuous scan mode, scanning speed of 8° min^{-1} and angle of 0.02° per scanning step. The characteristic 2θ peaks for each mineral phase are summarized in the Appendix.

4 RESULTS

4.1 Palaeomagnetic results

The NRM intensity of the FXG samples varies from 0.01 to 0.15 A m^{-1} and the directions are close to the present magnetic field ($D/I = 359/41.5°$; Fig. 2a), which indicates that the NRMs are overprinted to a significant degree. This was further confirmed by the stepwise thermal demagnetization. Most samples have one magnetic component and the characteristic remanent magnetization (ChRM) direction is generally resolved from 80 to 650/660 °C (Fig. 3); these samples are referred to as Type I. The Type I ChRM directions are better clustered in geographic coordinates with a mean direction of $D/I = 1/47°$, with $N = 10$, $n = 112$, $k = 440$ and $\alpha_{95} = 2.1°$ (Fig. 2b). Only a few samples have two magnetic components: a low-temperature component (LTC) was generally removed below 600 °C and the ChRM direction was resolved in the temperatures 610–660 °C (Fig. 4). These samples are referred to as Type II. The Type II LTC directions are clustered and fall close to the present magnetic field (Fig. 2c). After removing the LTC, the nine ChRM directions significantly depart from the present magnetic field and have mean direction of $D/I = 213/19°$ ($k = 16$, $\alpha_{95} = 11.7°$; Fig. 2c). Detailed palaeomagnetic results are given in Table 1.

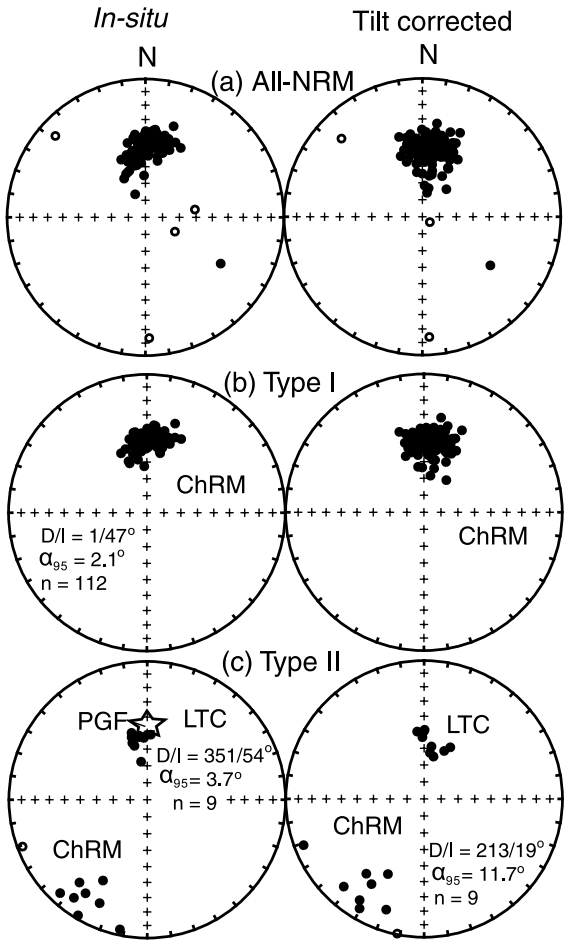

Figure 2. Equal-area projections of *in situ* and tilt-corrected (a) NRM directions, (b) Type I ChRM directions and (c) Type II ChRM and low temperature component (LTC) directions. Open (solid) circles represent lower (upper) hemisphere projection. The star denotes the present geomagnetic field (PGF).

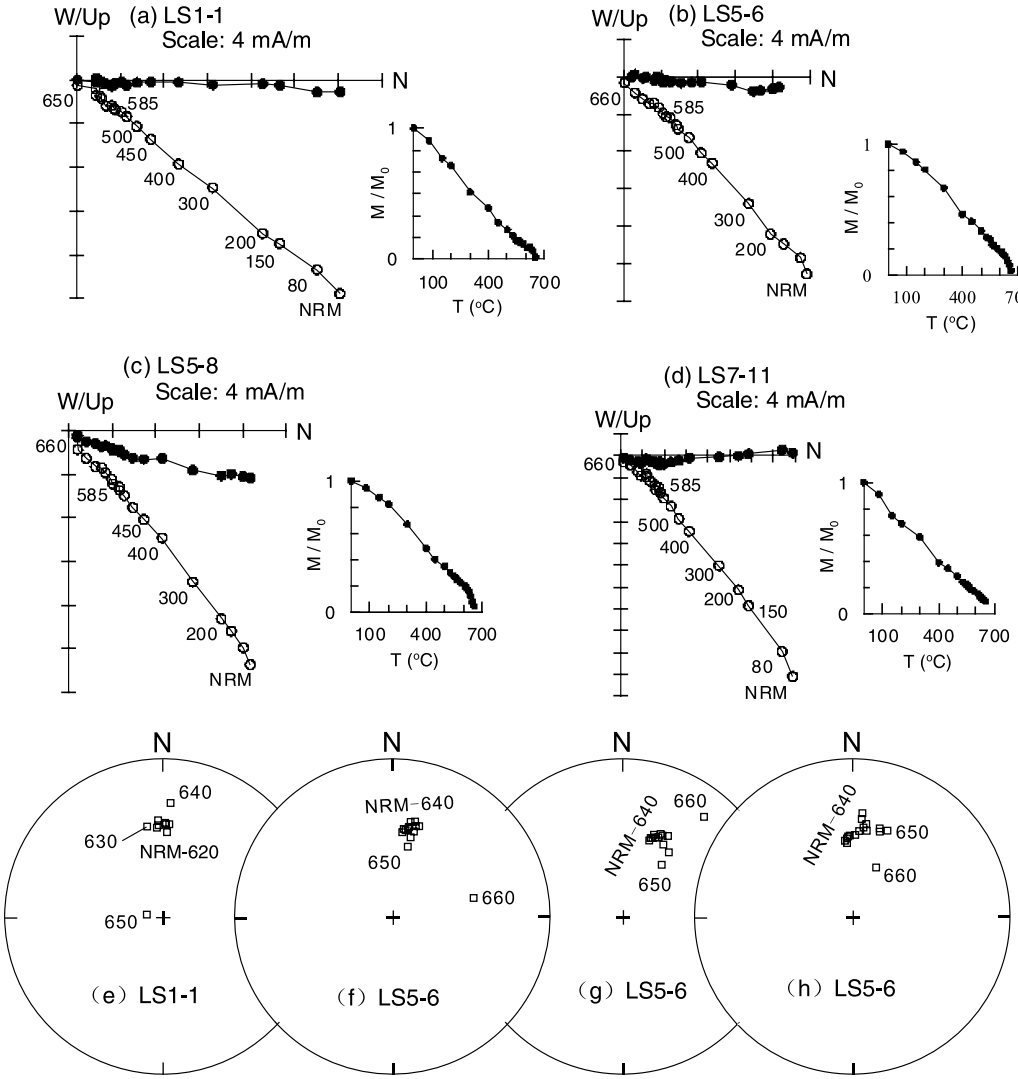

Figure 3. (a)–(d) Representative orthogonal plots of Type I thermal demagnetization (in geographic coordinates) for the Feixianguan Formation. The horizontal (vertical) component is marked with solid (open) circles. (e)–(h) Equal-area projections of the thermal demagnetization directions in lower hemisphere. Treatment temperatures are in degrees Celsius.

Applying the fold test to the ChRMs of Type I samples indicates the best grouping at 0 per cent unfolding (Fig. 2a). The corresponding palaeomagnetic pole (89.1°N, 331.7°E, $k = 338.2$, $A_{95} = 2.4°$) from Type I samples is coincident with the Quaternary–Palaeogene pole of the Yangtze Block (87.5°N, 315.6°E; Huang *et al*. 2008 and references therein), which suggests that these ChRMs were remagnetized in the late Cenozoic. The LTC directions of Type II samples fall close to the ChRM direction of Type I samples, both of which have better clustering in the geographic coordinates (Fig. 2c). This suggests that the palaeomagnetic directions recorded by the LTC of Type II samples also represent a late Cenozoic overprint. The virtual geomagnetic pole (VGP) of the mean ChRMs of Type II samples is 53.4°N, 216.6°E. The confidence level (α_{95} value of the mean Type II ChRM) of the VGP overlaps with the A_{95} circle surrounding the early Triassic palaeomagnetic pole of the SCB (45.7°N, 217.7°E; Enkin *et al.* 1992 and references therein; Fig. 5a), suggesting they are duplicate within 95 per cent confidence. In addition, this VGP is different from all more-recent pole positions of SCB (Fig. 5b), which suggests the ChRMs of Type II samples are primary.

4.2 Rock magnetic results

4.2.1 Anhysteretic remanent magnetizations (ARM), HIRM and S-ratio

HIRM values are about 20 times higher than ARM, which ranges from 0.02 to 0.16 $\times$ 10^{-3} $Am^2\,kg^{-1}$. This indicates that a high-coercivity mineral (haematite) is dominant and that low-coercivity minerals (magnetite and maghemite) are a rare minor component. Values of mass-normalized ARM and HIRM generally increase with increasing *S*-ratio and can be divided into two groups (Fig. 6): Samples with *S*-ratio >0.15 and those with *S*-ratio <0.15. All Type II samples fall into the *S*-ratio <0.15 group, which suggests that only samples with higher concentration of haematite could possibly keep the primary remanence. The *S*-ratios of Type I samples are widely distributed and fall into both categories, which indicates that the remagnetized samples have two types of mineralogy. To compare with the Type II samples, the Type I samples are further divided into two subgroups, Type I-1 with *S*-ratio <0.15 and Type I-2 with *S*-ratio >0.15. Further rock-magnetic investigation was aimed at

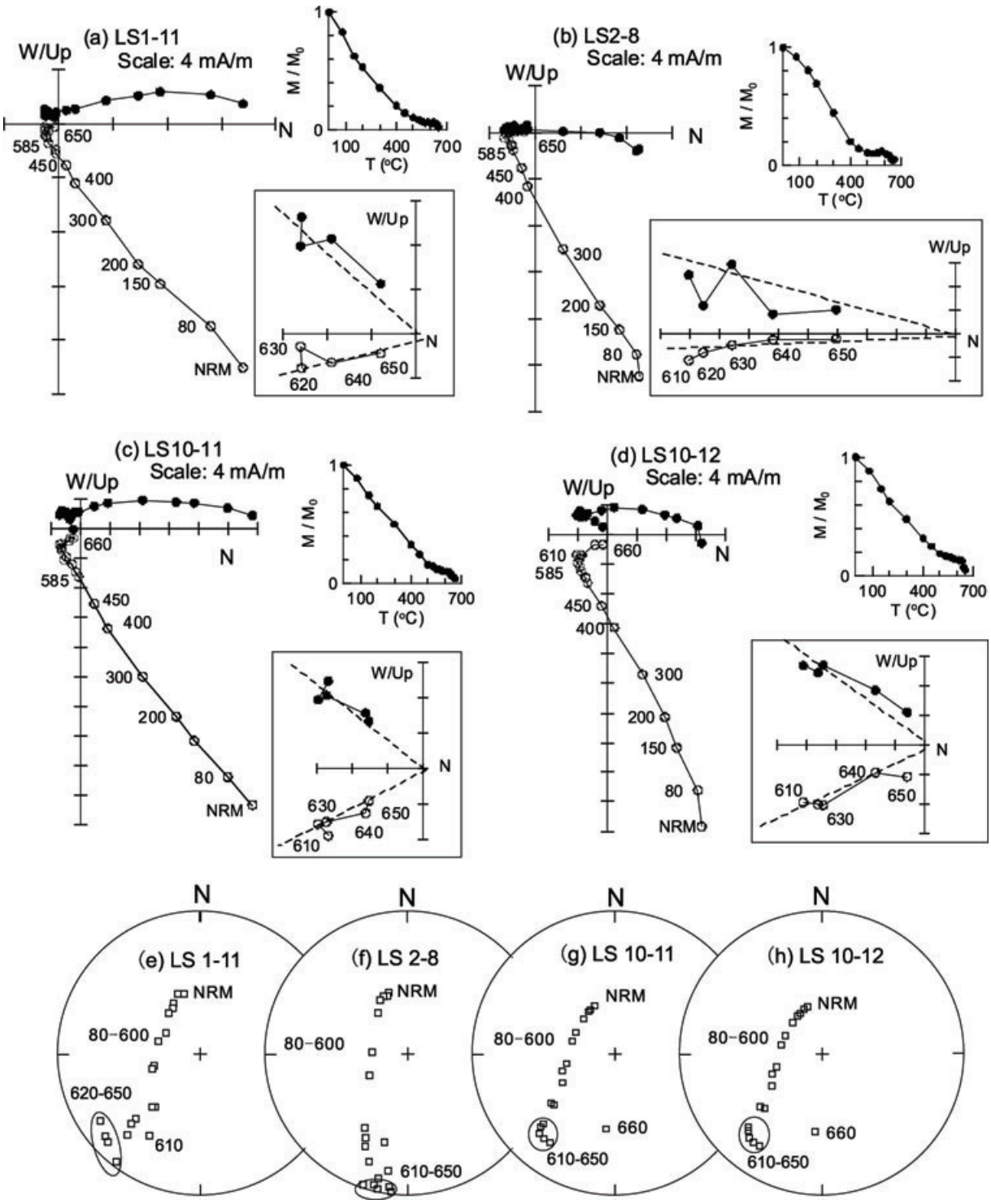

Figure 4. (a)–(d) Representative orthogonal plots of Type II thermal demagnetization for the Feixianguan Formation with two components. The square inset is an enlargement of the high-temperature section. Coordinates and symbols are the same as in Figure 3. (e)–(h) Equal-area projections of the thermal demagnetization directions in lower hemisphere. The symbols within the circles are used in the analysis of ChRM direction.

distinguishing the different mineralogy of these different types of samples.

4.2.2 Low-temperature magnetic measurements

Low-temperature magnetic measurements are an effective way to detect magnetic minerals. The thermal decay of SIRM acquired at 10 K indicates a significant loss of remanence around 120 K (Fig. 7), the Verwey transition, which indicates the presence of magnetite (Verwey *et al.* 1947). The first derivatives (dM/dT) of the thermal demagnetization curves of low-temperature remanence were calculated to better identify the changes during sample warming. This transition is much more pronounced in the dM/dT curves (Fig. 7). The low-temperature measurements, however, did not

Table 1. Palaeomagnetic directions and descriptive statistics from the Feixianguan samples.

Site/sample	*n*/*N*	Dg (°)	Ig (°)	Ds (°)	Is (°)	*k*/Temp	α_{95}/MAD (°)	Type
LS1	8/9	−2.5	46.8	3.7	43.4	208.7	3.4	I
LS2	9/9	−7.7	52.4	17.2	60.0	90.7	4.9	I
LS3	13/13	−3.1	45.1	−1.0	50.1	117.8	3.6	I
LS4	12/13	2.7	43.6	−5.9	43.5	209.8	2.8	I
LS5	11/12	8.7	46.9	2.9	50.0	105.9	4.1	I
LS6	12/13	−0.1	47.1	−6.6	47.3	261.1	2.5	I
LS7	13/13	2.8	46.7	5.9	47.6	130.4	3.4	I
LS8	12/12	3.0	43.5	13.4	48.0	121.6	3.7	I
LS9	11/12	1.8	46.0	16.8	49.5	276.6	2.5	I
LS10	11/11	2.0	47.2	8.9	41.6	111.9	4.0	I
Mean	112/116	0.9	46.6	5.2	48.4	440.2	2.1	
LS01–07	–	210.9	2.9	210.5	8.9	620–660 °C	14.4	II
LS01–10	–	208.7	33.8	205.7	39.5	610–650 °C	12.6	II
LS01–11	–	223.0	8.5	222.5	15.1	620–650 °C	11.6	II
LS02–02	–	249.4	−4.2	249.0	7.4	620–640 °C	7.4	II
LS02–03	–	216.8	12.5	212.5	14.3	610–650 °C	14.0	II
LS02–08	–	191.9	4.7	191.3	−0.8	610–650 °C	9.9	II
LS02–09	–	204.7	18.8	198.9	16.5	610–640 °C	13.4	II
LS10–11	–	219.3	23.7	217.7	32.2	610–650 °C	8.7	II
LS10–12	–	213.4	20.1	211.7	28.4	610–650 °C	9.5	II
Mean	9	215.4	13.9	213.3	18.6	16.0	11.7	

N (*n*), the number of the selected (measured) samples; Dg (Ds), Ig (Is), declination and inclination before (after) tilt correction; *k*/Temp, Fisher precision parameter of the mean directions from the Type I samples or the temperature interval selected for the linear fit for Type II samples; α_{95}/MAD, radius of the 95 per cent confidence circle about the mean direction for the Type I samples or mean angular deviation from the Type II samples.

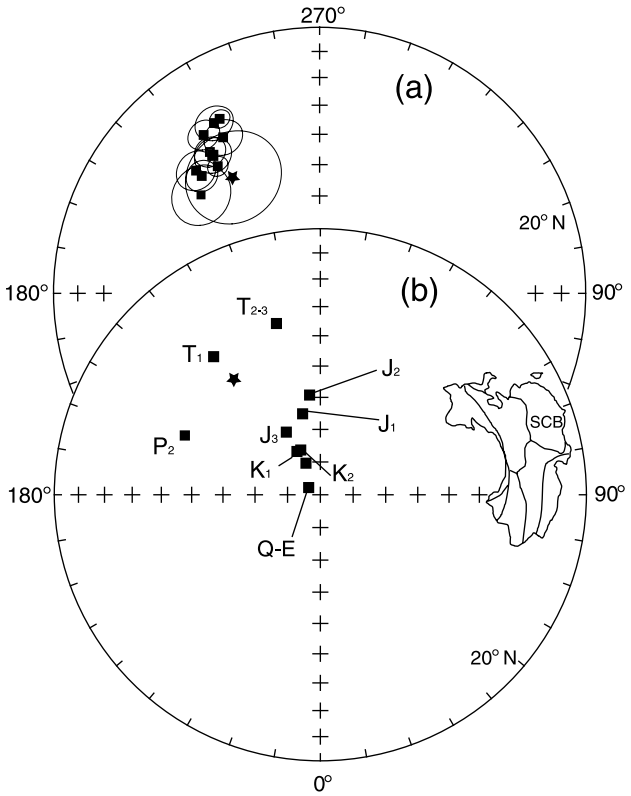

Figure 5. Equal-area projections in lower hemisphere of (a) the VGP from Type II ChRM (star) and the early Triassic palaeomagnetic poles (square) of the South China Block (SCB); (b) palaeomagnetic poles of SCB from Permian to present (Enkin *et al*. 1992 and references therein). The circles imply the 95 per cent confidence of the pole. P_2, late Permian; T_1/T_{2-3}, early/middle to late Triassic; $J_1/J_2/J_3$, early/middle/late Jurassic; K, Cretaceous; E, Palaeogene; Q, Quaternary.

highlight any significant differences between the different *S*-ratio samples.

4.2.3 $\chi-T$ curves

In general, the susceptibility (χ) drops at about 585 °C during the heating cycle (Figs 8a–c). This suggests that magnetite is a contributor to magnetic susceptibility, which is consistent with the low-temperature magnetic measurements (Fig. 7). The large residual magnetic susceptibility above 585 °C drops at ∼680 °C, the Néel temperature of haematite, which indicates the presence of a large amount of haematite. All three types of samples have significantly different $\chi-T$ features in argon compared with heating in air (Figs 8a-c). When in air, the room-temperature susceptibility generally decreases after heating; in contrast, it increases by a factor of at least 2 after heating in argon. All of the cooling curves in argon exhibit a distinctive Hopkinson peak at around 520 °C (Dunlop & Özdemir 1997), which may be the result of either the neoformation of the fine-grained magnetite from iron-bearing silicates/clays or the formation of magnetite by reduction of haematite (e.g. Hunt *et al*. 1995; Deng *et al*. 2000). The reversibility of the cooling and heating curves above 550 °C suggests that it is more likely caused by the former reason.

On the heating curve of some Type I-2 samples, there is a distinctive hump at around 300 °C, followed by a decrease of susceptibility (Fig. 8c). It could be interpreted as the conversion of metastable ferrimagnetic maghemite to antiferromagnetic haematite (Liu *et al*. 2005), which suggests that the mineralogy of Type I-2 samples may be variable. Sidertie is unlikely to be the source of the irreversibility. Because it starts breaking down to form very fine-grained magnetite on heating to 385–410 °C, and the process is complete by ∼450–600 °C (Pan *et al.* 2000), however, for our samples, χ increase starts at ∼140 °C, peaks at ∼300 °C and completes at ∼400 °C.

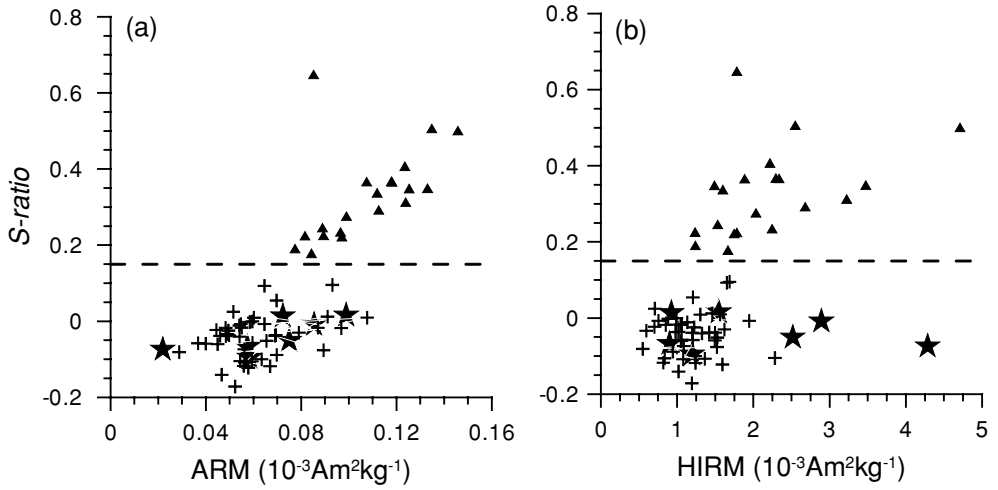

Figure 6. *S*-ratio versus (a) ARM and (b) HIRM for the studied samples. These samples can be divided into three groups: Type I-1, remagnetized with *S*-ratio < 0.15 (cross); Type I-2, remagnetized with *S*-ratio > 0.15 (triangle); and Type II with primary remanence (star).

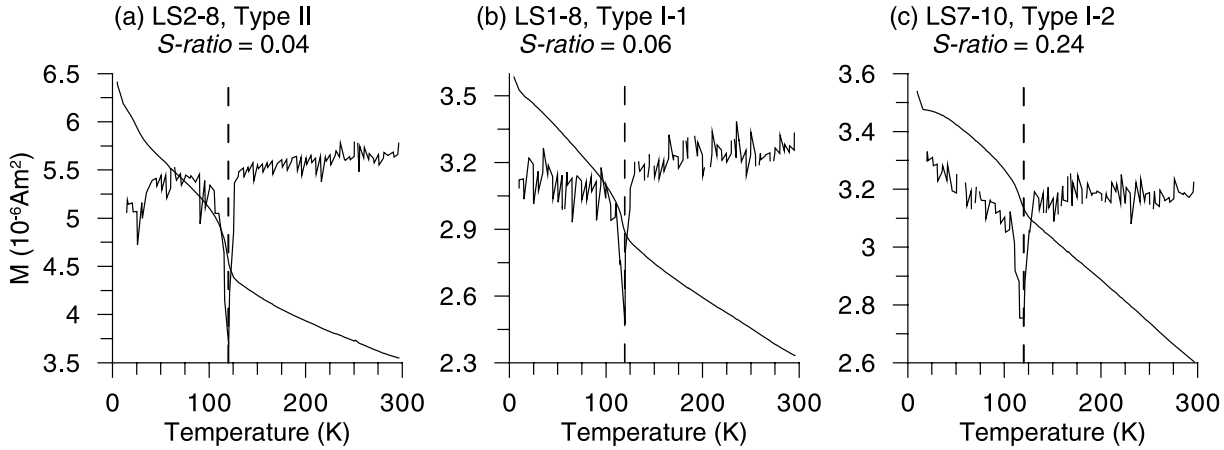

Figure 7. Representative low-temperature thermal demagnetization of the SIRM acquired at 10 K. The dashed lines are the first derivatives (d*M*/d*T*) of the thermal demagnetization curves, which indicate the Verwey transition at 120 K of magnetite (Verwey *et al*. 1947).

To further confirm the existence of maghemite in the Type I-2 samples, stepwise χ–T investigations in air are conducted on two representative samples (LS6–7 and LS7–10; Fig. 8d). Both of these samples were first heated to 400 °C and cooled to room temperature. Sample LS6–7 was then heated to 600 °C, but a fresh specimen of LS7–10 was used. The consistent behaviour of all the χ–T curves indicates that the two samples have common characteristic mineralogy. Furthermore, only the fresh samples have the distinctive humps at ∼350 °C not the pre-heated samples, which suggests that the maghemite is present in the samples.

Mixtures of representative natural samples of the three types (200 mg) with chlorite (20 mg) were heated in air and argon (Figs 8e and f, respectively). After heating–cooling in air, the mixtures did not exhibit significant differences with that of natural samples alone. However, when heated in argon, magnetic enhancement of LS1–7 (LS1–7+chlorite) is higher than that of LS1–6 (LS1–6+chlorite) and LS 6–7 (LS6–7+chlorite). The cooling curves of mixtures LS1–7+chlorite and LS1–6+chlorite are higher than the corresponding natural samples alone, which suggests that magnetic susceptibility enhancement upon heating in argon could be affected by the presence of chlorite. The susceptibility curve of LS6–7+chlorite is similar to that of LS6–7 alone, which suggests that the oxidation of chlorite may be further progressed in this sample.

4.2.4 Hysteresis properties

All studied samples have pronounced wasp-waisted hysteresis loops; however, the three different types of samples have different hysteresis parameters (Fig. 9). The wasp-waisted shapes arise from the coexistence of two different magnetic components with contrasting coercivities, such as the combination of low-coercivity magnetite and/or maghemite mixed with high-coercivity haematite and/or goethite (Roberts *et al*. 1995; Tauxe *et al*. 1996). In this study, the wasp-waisted loops are most probably due to the coexistence of haematite with magnetite and/or maghemite. The open nature of the hysteresis loops up to 0.6 T is further confirmation of the dominance of haematite in these samples. The wasp-waisted loops of the Type I-1, Type I-2 and Type II samples are likely the result of mixtures of haematite with magnetite alone, magnetite and maghemite or maghemite alone. Typically, loops of Type I-2 samples display the narrowest waist, with the lowest B_c (29.6–31.4 mT) and B_{cr} (127–197.2 mT) values (Figs 9g–i), comparatively, the other two types, Type II (Figs 9a–c) and Type I-1 (Figs 9d–f) samples have

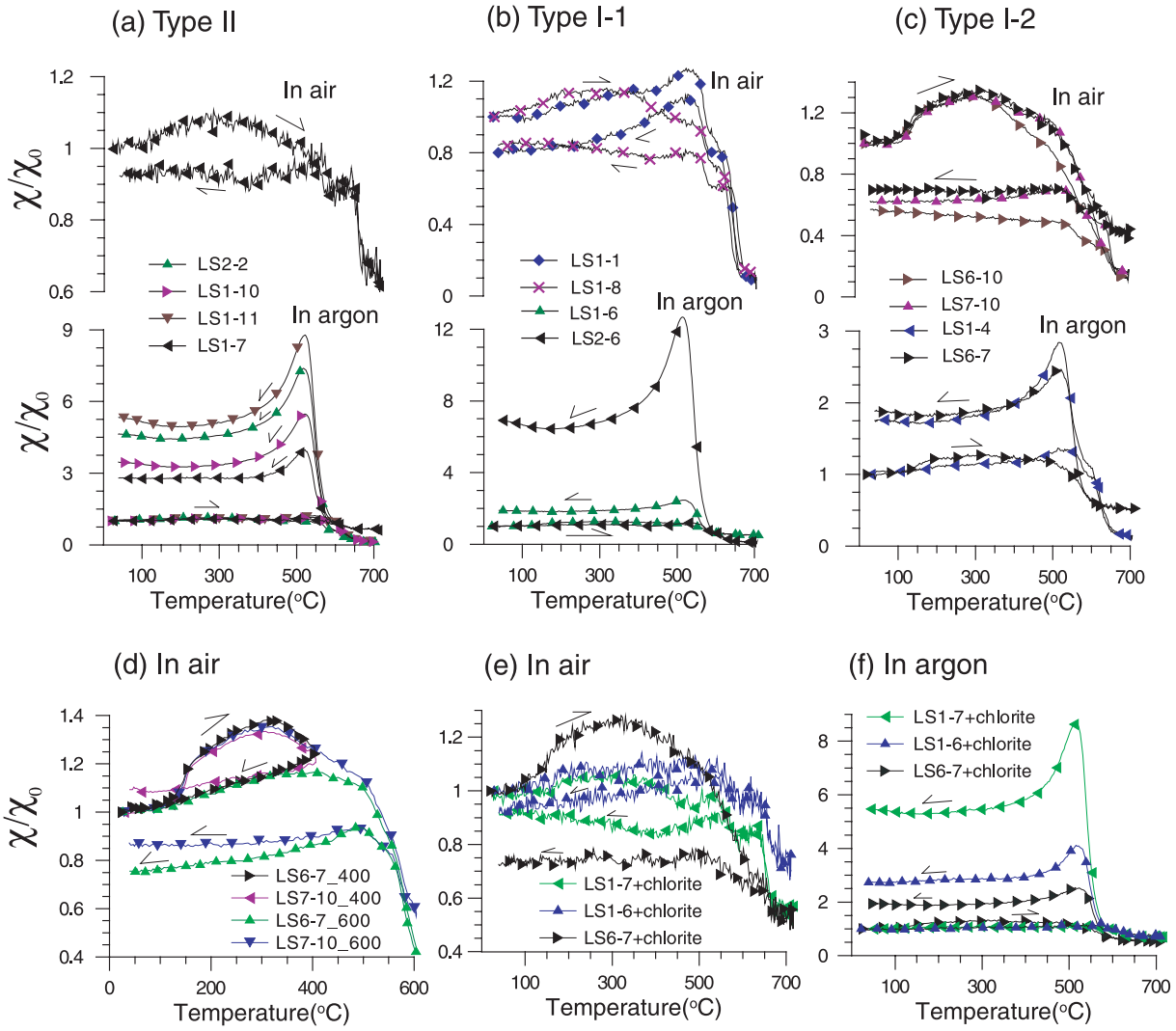

Figure 8. Representative magnetic susceptibility (normalized by room susceptibility) temperature ($\chi-T$) dependence curves. Representative (a) Type II, (b) Type I-1 and (c) Type I-2 samples during heating and cooling in air or in argon. (e) Stepwise $\chi-T$ measurements on two Type I-2 samples. $\chi-T$ curves of mixtures of representative natural Feixianguan samples with chlorite, measured in (d) air or in (f) argon. Arrows indicate the heating–cooling curves.

wider waists with larger B_c (47–98 mT) and B_{cr} (306–390 mT) values. This suggests that Type I-2 samples have relatively the most maghemite/magnetite with the least haematite, whereas, Type I-1 and Type II samples contain relatively more haematite.

Hysteresis parameters are also measured on one Type I-2 sample (LS7–10) that underwent stepwise $\chi-T$ measurement. After first 400 °C cycle, the B_c value decreased from 39.4 to 32.3 mT and the B_{cr} value increased from 197.2 to 276.8 mT, which indicates that after heated to 400 °C, the low-coercivity minerals in sample LS7–10 decreases and that of high-coercivity minerals increases. After heated to 600 °C, the B_c value remains unchanged (32.8 mT), but B_{cr} further increases to 481.7 mT, which indicates that the significant decrease of the low coercivity happens before 400 °C. This supports the suggestion that the humps at ∼300 °C are due to the maghemite in natural Type I-2 samples.

4.3 Mineralogy investigation

Microscope investigation is a quick and useful method to identify the mineral species and is essential for understanding the diagenetic processes of the rock. For the FXG samples, the shape of the opaque minerals, which would normally be more resisted to rounding, are rounder than the light-coloured minerals (Fig. 10a). This suggests a post-depositional recrystallization process. Given the coexistence of chlorite (Fig. 10b), this suggests the occurrence of low-grade metamorphism of the rock (Wei & Powell 2003).

XRD analysis (see Supporting Information) confirms the presence of significant amount of chlorite, haematite, quartz, plagioclase and calcite in the FXG Formation. The lack of the characteristic 2θ peaks of magnetite and maghemite further indicates that they are minor phases within the studied samples.

5 DISCUSSION

5.1 Formation process of the magnetic mineral phases

Red beds owe their distinctive colour to fine-grained, chemically produced haematite pigment. Larger black-specular haematite grains of detrital origin (Irving 1957; Van Houten 1968) are either derived from erosion of earlier red beds, volcanic terrains or formed by oxidation of magnetite during erosion and transport (Steiner 1983). For samples of the FXG Formation, the high temperature

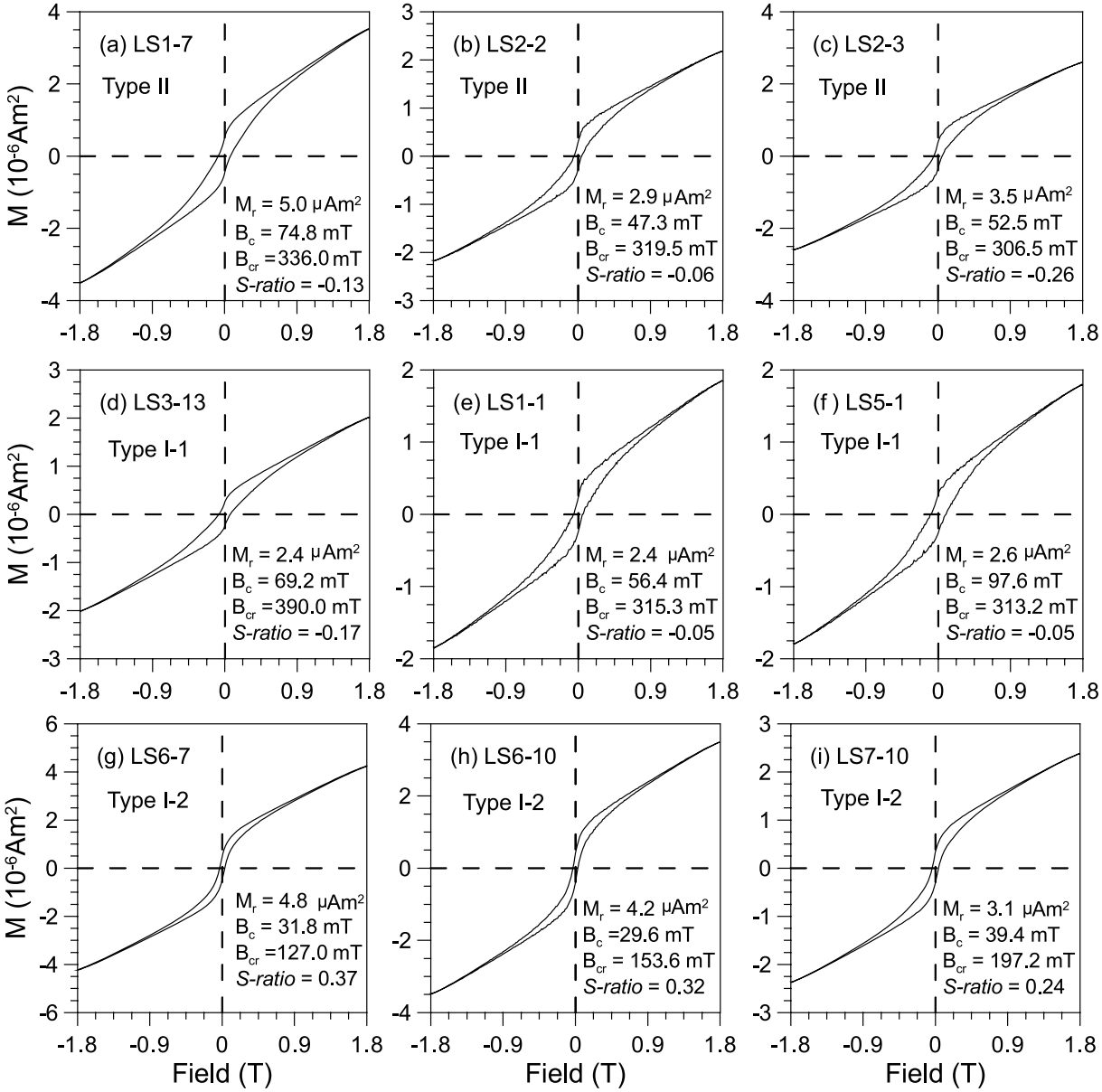

Figure 9. Representative hysteresis loops measured at room temperature without paramagnetic correction.

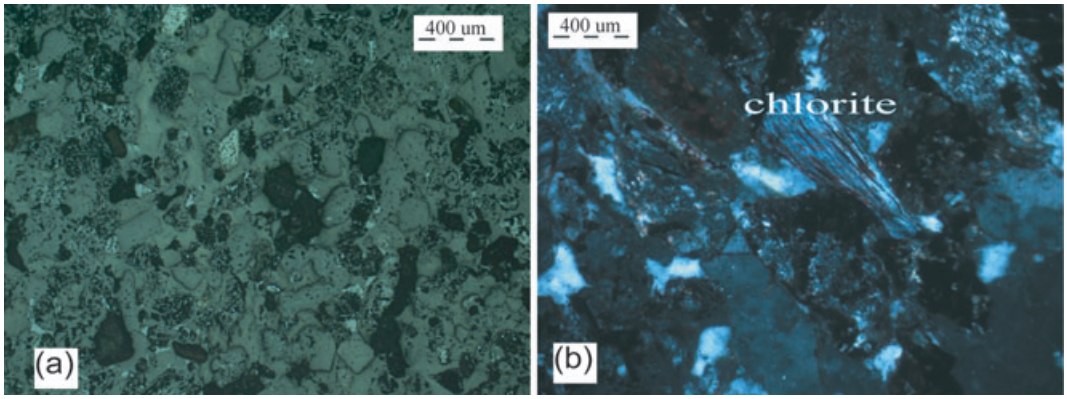

Figure 10. Representative microphotographs of FXG samples, (a) the opaque and light minerals (in reflected light) and (b) the presence of chlorite in the sample (in transmitted light).

component (HTC) of the Type II samples, which represents the primary remanence, is completely unblocked at 650 or 660 °C and is most likely carried by the detrital haematite.

Post-depositional dissolution of detrital magnetic minerals during and after burial tends to preferentially remove the fine-grained magnetic particles, and more intensive and prolonged dissolution may subsequently destroy the coarse-grained magnetic particles (e.g. Turner 1980; Karlin & Levi 1983; Snowball 1993; Tarduno 1994). Dissolution of magnetic minerals and iron oxides, and the release of Fe from silicates provide the Fe that reacts with other dissolved elements to subsequently yield new ferromagnetic minerals (Tarduno 1995; Rowan & Roberts 2006; Ao *et al*. 2010). A laboratory study indicated that the iron adsorbed onto the surface of smectite can lead to amorphous iron nanophases that convert to new ferromagnetic minerals above 250 °C (Hirt *et al*. 1993). In nature, during fluid migration iron nanophases may convert to magnetite and further oxidize to maghemite and finally haematite (e.g. Turner 1980; Dunlop & Özdemir 1997).

In this study, the LTC of Type II samples and the ChRM of Type I samples are both overprints due to a late Cenozoic magnetic field. It is reasonable to conclude that the secondary magnetic minerals are authigenic haematite and maghemite. The XRD spectra of the FXG samples indicate the presence of a significant amount of chlorite, which may adsorb the iron and lead to iron nanophases that can convert to magnetite. The $\chi - T$ curves of the natural and mixture samples in argon (Fig. 8) suggest that in nature haematite could be reduced to magnetite during heating in a low-oxygen environment in the presence of chlorite. The different $\chi - T$ features in air and argon also suggest that the chemical transformation of magnetic minerals during thermal treatment occurs exclusively in a low-oxygen environment. Zhang *et al.* (2012) showed that the presence of all three components (haematite, chlorite and a low-oxygen atmosphere) is necessary to induce a reduction of haematite to magnetite.

Previous studies have indicated that the threshold between single-domain (SD) and multidomain haematite could be on the order of tens of μm (Dunlop & Özdemir 1997). Most haematite particles in natural samples are, therefore, within the stable SD region, which is the main reason that the CRM carried by the secondary haematite is stable. However, the coercivity of SD haematite varies significantly with respect to the grain size distribution. Generally, with increasing grain size of haematite particles, the coercivity increases (Liu *et al*. 2007). As a result of continuous grain growth, this newly formed haematite will have a broad unblocking temperature spectrum. It is common for haematite formed in solution to have a degree of Al substitution, which can further complicate the magnetic properties of haematite. The combined effects of grain size and Al substitution can result in the unblocking temperatures of secondary haematite varying significantly (Liu *et al*. 2007). The secondary magnetizations in our samples (the ChRM of Type I samples and LTC of Type II samples) have broad unblocking spectra, whereas, the primary magnetization, which resides in the HTC of Type II samples, have different unblocking spectra. Therefore, the primary NRM can be either fully or partially remagnetized depending on whether the maximum unblocking temperature of the secondary haematite can reach that of the detrital haematite.

Maghemite is also a carrier of the LTC for the Type II samples. Previous work has suggested a T_c of 645 °C for synthetic maghemite (Özdemir 1990) and 610 °C for natural maghemite (de Boer & Dekkers 1996). However, in natural environments, especially pedogenic environments, newly formed maghemite usually contains a higher amount of imperfections and is under higher degrees of strain, which can significantly decrease T_c (de Boer & Dekkers 1996). In addition, substitution of Fe by Al can further lower the T_c of maghemite (da Costa *et al*. 1995). Therefore, for our samples, where the maghemite formed in a natural environment, it is less likely to be the dominant carrier for the LTC of the FXG samples due to its potential lower T_c. Fine-grained maghemite is thermally unstable and our thermomagnetic analyses indicate the presence of a thermally unstable component (e.g. Fig. 8a). Similarly, the high coercivity of the bulk sample indicates that low-coercivity components, such as maghemite, are not dominant.

The remagnetization process for our studied samples can be summarized as follows. Initially, the relatively coarse-grained haematite and magnetite of detrital origin were deposited during the early Triassic. These two minerals carried the primary detrital remanent magnetization (DRM). During the Quaternary–Palaeogene period, the region went through a fluid event that accelerated the neoformation of fine-grained haematite and maghemite with variable unblocking temperature spectra. These newly formed magnetic minerals, particularly the haematite, carry the secondary CRM, which fully or partially contaminated the primary DRM. The degree of overprinting was controlled by the distribution of unblocking temperatures. This region was uplifted at the same time as the Tibetan plateau to the northwest as the result of the India–Eurasia collision during the early Palaeogene (e.g. Wang *et al*. 1998; Dupont-Nivet *et al*. 2008; Najman *et al*. 2010). This uplift of the Tibetan plateau could have been responsible for the fluid migration that instigated the formation of the authigenic maghemite and haematite.

5.2 Implications for palaeomagnetic research

Although most of our samples have been remagnetized, the small number of samples (~7 per cent) for which the HTC is uncontaminated, can still be used to define the PRM. The *S*-ratio value is proved to be a useful pre-selection criterion to eliminate the fully remagnetized samples, for example, the samples with *S*-ratio >0.15 are remagnetized. This is a quick-to-measure parameter that can be applied when studying red bed samples. In addition, the χ–T behaviour is also useful to identify the remagnetized samples, for example, the samples that contain maghemite are fully remagnetized. Hysteresis parameters are also indicative. Microscope investigation has proven to be an effective method that can give indication of mineral diagenetic changes, which could give insight into the remagnetization process. Therefore, we suggest petrographic studies on representative samples before palaeomagnetic and rock–magnetic experiments. Combined with the microscopy investigation, *S*-ratio and χ-T experiments will not only increase the success rate of recovering the primary remanence, but also make it feasible to obtain reliable palaeomagnetic pole for red beds, such as the FXG Formation. On the other hand, the combined study of the palaeomagnetic and rock magnetic investigations could be extended to other studies to reveal the CRM remagnetization mechanism.

6 CONCLUSIONS

On the basis of the discussion above, we conclude that most of our studied samples from the Lower Triassic FXG Formation in southwest China have been remagnetized due to the authigenic haematite and maghemite. This authigenic haematite has a broad-blocking temperature (T_b) distribution. When the spectrum of T_b for the authigenic haematite is close to that of the detrital haematite, the PRM will be completely remagnetized. In contrast, when the

concentration of the authigenic haematite is relatively low, there is a chance that its maximum T_b (in this study ~610 °C) is lower than that of the detrital component. The PRM carried by these samples (<7 per cent) can still be isolated at elevated temperatures (>610 °C).

This work indicates the authigenic haematite and maghemite could be formed in a short time when fluid is involved, which could overprint the PRM significantly. The concentration and properties (e.g. the T_b) of the authigenic haematite are key mechanisms of the remagnetization process and dictate the extent to which the PRM is overprinted. Our study emphasizes the usefulness of petrographic investigation and rock magnetic methods, especially the *S*-ratio value, for pre-selecting samples suitable for retrieving the PRM.

ACKNOWLEDGMENTS

The author's are very grateful to J. Y. Yin and S. J. He for assistance in the field, and to X. Y. Zhao for assistance with some experiments. We also thank Professor K. Ye for assistance with the microscopy work and Dr. Greig A. Paterson for revising the manuscript. We also wish to thank Andy Biggin, Phil Schmidt and Roberto Molina Garza for their helpful suggestions and comments on the manuscript. This work was supported by the NSFC (40821091, 40974036) and Chinese Academy of Sciences. QL further thanks the supports from the '100 Talent Program' of CAS.

REFERENCES

Ao, H., Deng, C.L., Dekkers, M.J. & Liu, Q.S., 2010. Magnetic mineral dissolution in Pleistocene fluvio-lacustrine sediments, Nihewan Basin (North China), *Earth planet. Sci. Lett.,* **292,** 191–200.

Bai, L.X., Zhu, R.X., Wu, H.N. & Guo, B., 1998. Remagnetization history of Middle Triassic Leikoupo formation on Wangcang section in Sichuan Province, China (in Chinese with English absract), *Sci. China (Ser. D),* **28,** 63–68.

Collinson, D., 1967. Chemical demagnetization, in *Methods in Paleomagnetism,* pp. 159–162, eds Collison, D.W., Creer, K. M. & Runcorn, S.K., Elsevier, Amsterdam.

Cornell, R.M. & Schwertmann, U., 2003. *The Iron Oxides: Structure, Properties, Reactions, Occurrences, and Uses,* 2nd edn, pp. 413–415, Wiley-VCA Verlag GmbH & Co. KGaA, Weinheim.

da Costa, G.M., DeGrave, E., de Bowen, L.H., Bakker, P.M.A. & Vandenberghe, R.E., 1995. Temperature dependence of the hyperfine parameters of maghemite and Al-substituted maghemites, *Phys. Chem. Miner.,* **22,** 178–185.

de Boer, C.B. & Dekkers, M.J., 1996. Grain-size dependence of the rock magnetic properties for a natural maghemite, *Geophys. Res. Lett.,* **23,** 2815–2818.

Deng, C.L., Zhu, R.X., Verosub, K.L., Singer, M.J. & Yuan, B.Y., 2000. Paleoclimatic significance of the temperature-dependent susceptibility of Holocene loess along a NW-SE transect in the Chinese loess plateau, *Geophys. Res. Lett.,* **27,** 3715–3718.

Dobson, J. & Heller, F., 1992. Remagnetization in southeast China and collision and suturing of the Huanan and Yangtze Blocks, *Earth planet. Sci. Lett.,* **111,** 11–21.

Dunlop, D.J., & Özdemir, Ö., 1997. *Rock Magnetism: Fundamentals and Frontiers,* Cambridge University Press, United Kingdom.

Dupont-Nivet, G., Dai, S., Fang, X., Krijgsman, W., Erens, V., Reitsma, M. & Langereis, C., 2008. Timing and distribution of tectonic rotations in the northeastern Tibetan Plateau, in *Investigations Into the Tectonics of the Tibetan Plateau,* pp. 73–87, eds Burchfiel, B.C., & Wang E., The Geological Society of America, Inc., USA.

Enkin, R.J., Yang, Z., Chen, Y. & Courtillot, V., 1992. Paleomagnetic constraints on the geodynamic history of the major blocks of China from the Permian to the present, *J. geophys. Res.,* **97,** 13 953–13 989.

Fisher, R., 1953. Dispersion on a sphere, *Proc. R. Soc. London A, Math. Phys. Sci.,* **217,** 295–305.

Gilder, S., Chen, Y. & Sen, S., 2001. Oligo-Miocene magnetostratigraphy and rock magnetism of the Xishuigou section, Subei (Gansu Province, western China) and implications for shallow inclinations in central Asia, *J. geophys. Res.,* **106,** 30 505–30 521.

Heller, F., Lowrie, W., Huamei, L. & Junda, W., 1988. Magnetostratigraphy of the Permo-Triassic boundary section at Shangsi (Guangyuan, Sichuan Province, China), *Earth planet. Sci. Lett.,* **88,** 348–356.

Hirt, A.M., Banin, A. & Gehring, A.U., 1993. Thermal generation of ferromagnetic minerals from iron-enriched smectites, *Geophys. J. Int.,* **115,** 1161–1168.

Huang, K.N., & Opdyke, N.D., 1996. Severe remagnetization revealed from Triassic platform carbonates near Guiyang, Southwest China, *Earth planet. Sci. Lett.,* **143,** 49–61.

Huang, B., Zhou, Y. & Zhu, R., 2008. Discussions on Phanerozoic evolution and formation of continental China, based on paleomagnetic studies (in Chinese), *Earth Sc. Front.,* **15,** 348–359.

Hunt, C.P., Banerjee, S.K., Han, J., Solheid, P.A., Oches, E., Sun, W. & Liu, T., 1995. Rock-magnetic proxies of climate change in the loess-palaeosol sequences of the western Loess Plateau of China, *Geophys. J. Int.,* **123,** 232–244.

Irving, E., 1957. The origin of the paleomagnetism of the Torridonian sandstones of north-west Scotland, *Phil. Trans. R. Soc. Lond. A, Math. Phys. Sci.,* **250,** 100–110.

Jones, C.H., 2002. User-driven integrated software lives: paleomag paleomagnetics analysis on the Macintosh, *Comput. Geosci.,* **28,** 1145–1151.

Karlin, R. & Levi, S., 1983. Diagenesis of magnetic minerals in recent haemipelagic sediments, *Nature,* **303,** 327–330.

Kent, D.V., Zeng, X.S., Zhang, W.Y. & Opdyke, N.D., 1987. Widespread Late Mesozoic to recent remagnetization of Paleozoic and Lower Triassic sedimentary rocks from south China, *Tectonophysics,* **139,** 133–143.

King, J.W. & Channell, J.E.T., 1991. Sedimentary magnetism, environmental magnetism and magnestostratigraphy, *Rev. Geophys.,* **29,** 358–370.

Kirschvink, J.L., 1980. The least-squares line and plane and the analysis of palaeomagnetic data, *Geophys. J. R. astr. Soc.,* **62,** 699–718.

Liu, Q.S., Deng, C.L., Yu, Y., Torrent, J., Jackson, M.J., Banerjee, S.K. & Zhu, R.X., 2005. Temperature dependence of magnetic susceptibility in an argon environment: implications for pedogenesis of Chinese loess/palaeosols, *Geophys. J. Int.,* **161,** 102–112.

Liu, Q.S., Roberts, A.P., Torrent, J., Horng, C.S. & Larrasoana, J.C., 2007. What do the HIRM and S-ratio really measure in environmental magnetism? *Geochem. Geophys. Geosyst.,* **8,** Q09011, doi:09010.01029/02007GC001717.

Ma, X.H. & Zhang, Z., 1989. Palaeomagnetic study of Permian rocks from Sichuan Emei region and Shanxi Taiyuan region (in Chinese), *Acta geophys. Sin.,* **32,** 451–465.

McCabe, C. & Elmore, R.D., 1989. The occurrence and origin of late Paleozoic remagnetization in the sedimentary rocks of North America, *Rev. Geophys.,* **27,** 471–494.

Najman, Y. *et al*., 2010. Timing of India-Asia collision: geological, biostratigraphic, and palaeomagnetic constraints, *J. geophys. Res.,* **115,** B12416, doi:10.1029/2010JB007673.

Özdemir, Ö., 1990. High-temperature hysteresis and thermoremanence of single-domain maghemite, *Phys. Earth planet. Inter.,* **65,** 125–136.

Pan, Y., Zhu, R., Banerjee, S.K., Gill, J. & Williams, Q., 2000. Rock magnetic properties related to thermal treatment of siderite: behavior and interpretation, *J. geophys. Res.,* **105,** 783–794.

Roberts, A.P., Cui, Y. & Verosub, K.L., 1995. Wasp-waisted hysteresis loops: mineral magnetic characteristics and discrimination of components in mixed magnetic systems, *J. geophys. Res.,* **100,** 17 909–17 924.

Rowan, C.J. & Roberts, A.P., 2006. Magnetite dissolution, diachronous greigite formation, and secondary magnetizations from pyrite oxidation: unravelling complex magnetizations in Neogene marine sediments from New Zealand, *Earth planet. Sci. Lett.,* **241,** 119–137.

Snowball, I.F., 1993. Geochemical control of magnetite dissolution in subarctic lake sediments and the implications for environmental magnetism, *J. Quat. Sci.,* **8,** 339–346.

Steiner, M.B., 1983. Detrital remanent magnetization in hematite, *J. geophys. Res.,* **88,** 6523–6539.

Steiner, M.B., Ogg, J., Zhang, Z. & Sun, S., 1989. The Late Permian/Early Triassic magnetic polarity time scale and plate motions of South China, *J. geophys. Res.,* **94,** 7343–7363.

Tarduno, J.A., 1994. Temporal trends of magnetic dissolution in the pelagic realm: gauging paleoproductivity? *Earth planet. Sci. Lett.,* **123,** 39–48.

Tarduno, J.A., 1995. Superparamagnetism and reduction diagenesis in pelagic sediments: enhancement or depletion? *J. geophys. Res.,* **22,** 1337–1340.

Tauxe, L., 2010. *Essentials of Paleomagnetism,* University of California Press, London.

Tauxe, L., Mullender, T. & Pick, T., 1996. Potbellies, wasp-waists, and superparamagnetism in magnetic hysteresis, *J. geophys. Res.,* **101,** 571–583.

Thompson, R. & Oldfield, F., 1986. *Environmental Magnetism,* Allen and Unwin, London.

Turner, J.S., 1980. Buoyancy effects in fluids. Cambridge University Press, New York.

Van Houten, F.B., 1968. Iron oxides in red beds, *Bull. geol. Soc. Am.,* **79,** 399–416.

Verwey, E.J., Haayman, P.W. & Romeijn, F.C., 1947. Physical properties and cation arrangement of oxides with spinel structures II. Electronic conductivity, *The J. Chem. Phys.,* **15,** doi:10.1063/1.1746466.

Walker, T.R., Larson, E.E. & Hoblitt, R.P., 1981. Nature and origin of hematite in the Moenkopi Formation (Triassic), Colorado Plateau: a contribution to the origin of magnetism in red beds, *J. geophys. Res.,* **86,** 317–333.

Wang, E., Burchfiel, B.C., Chen, L., Chen, J., Li, W. & Chen, Z., 1998. Late Cenozoic Xianshuihe-Xiaojiang, Red River, and Dali fault systems of southwestern Sichuan and central Yunnan, China, *Geol. Soc. Am. Special Paper,* **327,** 1–109.

Wang, Z. & Van der Voo, R., 1993. Pervasive remagnetization of paleozoic rocks acquired at the time of mesozoic folding in the South China Block, *J. geophys. Res.,* **98,** 1729–1741.

Wei, C. & Powell, R., 2003. Phase relations in high-pressure metapelites in the system KFMASH (K_2O–FeO–MgO–Al_2O_3–SiO_2–H_2O) with application to natural rocks, *Contrib. Mineral. Petrol.,* **145,** 301–315.

Zhang, C.X., Paterson, G.A. & Liu, Q.S., 2012. A new mechanism for the magnetic enhancement of hematite during heating: the role of clay minerals. *Stud. geophys. Geod.,* **56,** doi:10.1007/s11200-011-0018-1, in press.

Zijderveld, J.D.A., 1967. AC demagnetization of rocks: analysis of results, in *Methods in Paleomagnetism,* pp. 254–286, eds Collison, D.W., Creer, K.M. & Runcorn, S.K., Elsevier, New York.

APPENDIX

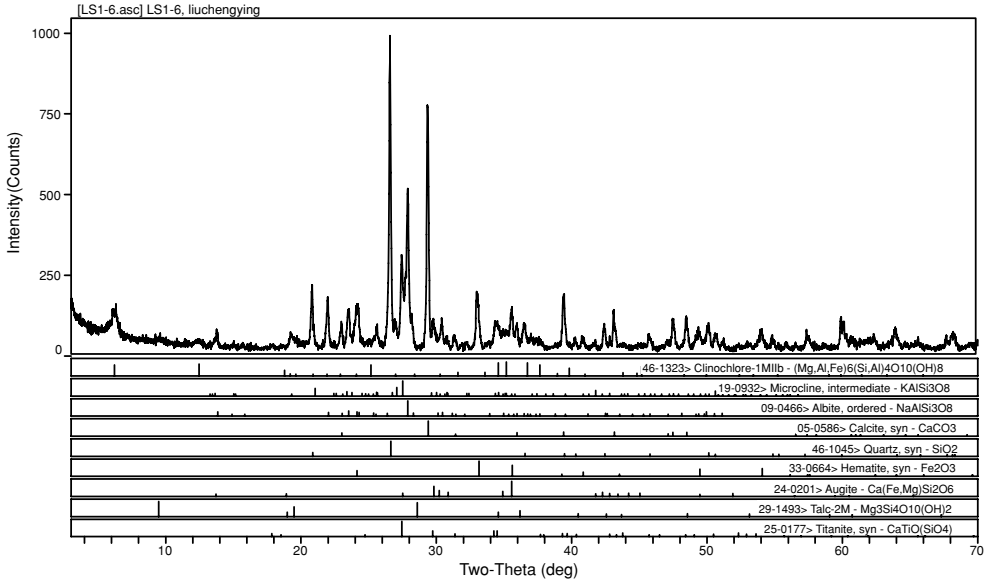

Figure A1. The characteristic 2θ peaks for each mineral phase.

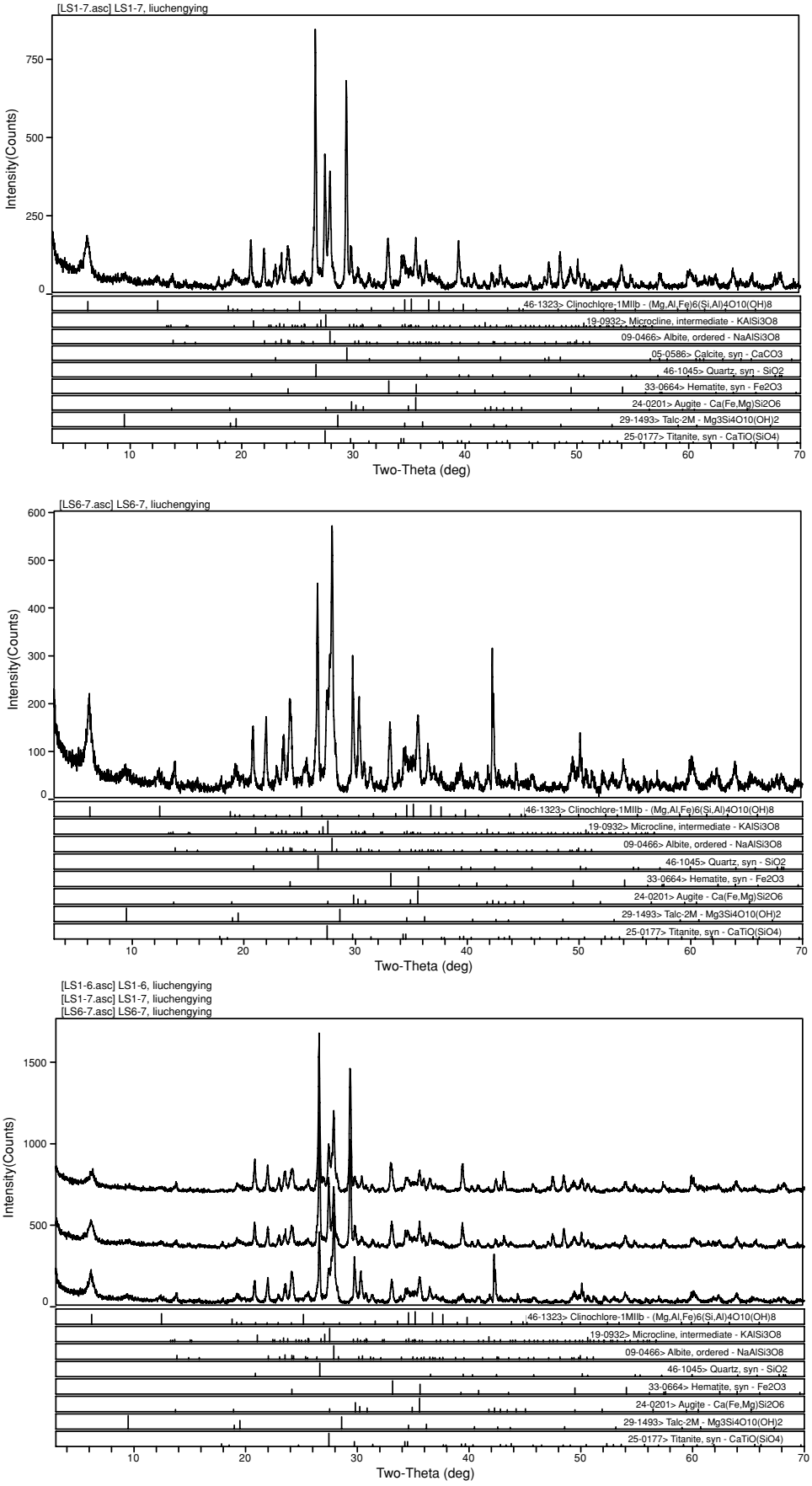

Figure A1. (*Continued.*)